Model Predictive Active Thermal Control Strategy for Lifetime Extension of a 3L-NPC Converter for UPS Applications

Novak, Mateja; Blaabjerg, Frede

Published in:
2020 IEEE 21st Workshop on Control and Modeling for Power Electronics (COMPEL)

DOI (link to publication from Publisher):
10.1109/COMPEL49091.2020.9265807

Publication date:
2020

Document Version
Accepted author manuscript, peer reviewed version

Model Predictive Active Thermal Control Strategy for Lifetime Extension of a 3L-NPC Converter for UPS Applications

Mateja Novak
Department of Energy Technology
Aalborg University
Aalborg, Denmark
nov@et.aau.dk

Frede Blaabjerg
Department of Energy Technology
Aalborg University
Aalborg, Denmark
fbl@et.aau.dk

***Abstract*—The neutral point clamped (NPC) converter topology suffers from unequal thermal stress distribution of the power devices, which limits the maximum output power of the converter and also reduces the lifetime. By applying a control strategy that can maintain an equal stress distribution between the inner and outer devices, the lifetime of the converter can be prolonged. In this paper, positive effects of a predictive active thermal control strategy on the lifetime of the NPC converter are presented applied for an uninterruptible power supply (UPS) application. A mission profile based lifetime is estimated for a typical UPS loading profile. The obtained results show that for the presented application the control algorithm can maintain the difference between the inner and outer device junction temperature within 1°C. Thus, the converter lifetime can almost be doubled by using the predictive active thermal control strategy. Moreover, a comparison of estimated B_1 lifetime for different mission profiles is also presented to illustrate how different ratings of the nominal and standby load affect the converter lifetime.**

***Index Terms*—Active thermal control, finite-set model predictive control, lifetime, neutral point clamped converter, reliability.**

I. Introduction

The design for reliability (DfR) has received a lot of attention in the past years in power electronic converter design. In order to improve the reliability of a power electronic converter system, the reliability of the components that are most prone to fail need to be increased. Typically, components that have the highest failure rate, are the semiconductor devices and the capacitors [1]. In this paper we will focus on the semiconductor failures. Thermal cycling is one of the most significant stressors of the devices. For the converter topologies that have multiple devices like multilevel or multi-cell topologies, the lifetime of the converter will be limited by the most stressed device. Therefore, it is quite clear that improvement of the thermal stress distribution will have a positive effect on the lifetime of the devices and thereby the whole converter system. This paper aims to investigate how large this impact is on an UPS application.

One of the topologies, where this uneven distribution is very pronounced, is the neutral point clamped topology (NPC). The schematics of the topology can be seen in Fig. 1. Due to the uneven stress distribution of the inner and outer devices, the lifetime of one pair of the devices is expected to be much lower due to the higher applied thermal stress [2]. Many different control strategies based on traditional linear or more advanced non-linear control algorithms were proposed to improve the stress distribution [3]–[6]. In our case study, the selected algorithm is based on model predictive control (MPC). The algorithm offers a very simple implementation in the state-of art control platforms and can use the three control objectives that are necessary for efficient and reliable operation of the NPC converter in UPS applications: voltage control, DC-link voltage balancing and thermal stress balancing.

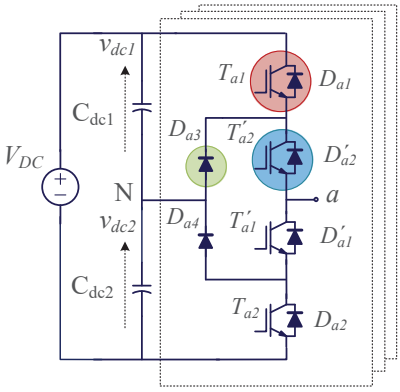

Fig. 1: Three level neutral point clamped converter topology.

Most lifetime analysis for NPC converters were performed for traditional linear controllers based on PWM [7] or using constant failure rate models from various handbooks like the Military-Handbook-217F [8], [9]. While some of them give a valuable insight into evaluating the redundancies of the three level (3L) converters like NPC and active NPC, it needs to be mentioned that lifetime assessment based on experience-based handbooks has been proven inaccurate because it is too general and it is not application specific [1]. A mission profile oriented lifetime estimation can avoid these drawbacks and give a more clear picture about the expected stress conditions

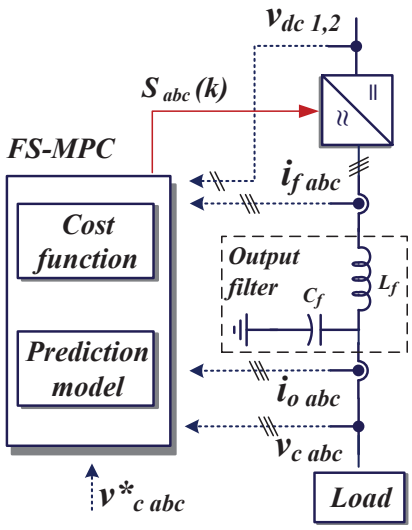

Fig. 2: System model of a finite-set (FS) MPC controlled three level NPC converter in standalone application.

TABLE I: Parameters of a finite-set MPC controlled three level NPC converter in standalone application.

Parameter	Value
Output voltage	400 V, 50 Hz
DC-link voltage	700 V
Output filter	15 μF, 2.4 mH
Nominal power	53 kW
Control algorithm sampling time	25 μs
Mission profile sampling time	60 s
IGBT module	650 V/150 A

for different applications as shown in [10] for industrial rolling mill application, in [11] for a PV application and in [12] for a wind turbine application.

In this case study, a typical UPS mission profile [13] is selected for evaluation of the semiconductor device thermal stress. It needs to be mentioned that a MPC based algorithm has not yet been used for extending and estimating the lifetime of the NPC converter in power electronic applications. In the next sections, the implemented control strategy will be explained, followed by a thermal stress analysis. The lifetime estimation process and obtained unreliability functions of the NPC converter are presented in the last section of the paper.

II. Control Strategy

The control strategy used in this case study was proposed in [14] and its schematic is shown in Fig. 2. It is a finite-set model predictive control (FS-MPC) based control strategy. The operating principle of the control strategy is straightforward. In each sample time the cost function, which describes the desired behaviour of the converter, will be evaluated for all possible switching states that can be applied to the 3L-NPC topology in order to find the one with minimum cost function values. The effects of each switching state on the converter output and load currents (i_f, i_o) and DC-link capacitor and load voltages (v_{dc}, v_c) are calculated using a discrete system model in $\alpha\beta$ stationary frame:

$$v_{dc1,2}(t) = C_{dc1,2}\frac{di_{dc1,2}(t)}{dt} \quad (1)$$

$$i_{f\,\alpha\beta}(t) = C_f\frac{dv_{c\,\alpha\beta}(t)}{dt} + i_{o\,\alpha\beta}(t) \quad (2)$$

$$v_{i\,\alpha\beta}(t) = L_f\frac{di_{f\,\alpha\beta}(t)}{dt} + v_{c\,\alpha\beta}(t) \quad (3)$$

where L_f and C_f are output filter inductance and capacitance, v_i is the inverter output voltage, $C_{dc1,2}$ is the capacitance of the DC-link capacitors and $i_{dc1,2}$ are the capacitor currents. Three objectives are included in the cost function: the load voltage control, DC-link voltage balancing and the active thermal control (ATC) to establish an even thermal distribution among the inner (T'_{x1}, T'_{x2}) and outer power devices (T_{x1}, T_{x2}) (see Fig. 1):

$$g = (v_c^* - v_c^P)^2 + \lambda_{dc}(v_{dc1}^P - v_{dc2}^P)^2 + \lambda_t g_t \quad (4)$$

$$g_t = |I_{fa}(k)| \cdot n_a + |I_{fb}(k)| \cdot n_b + |I_{fc}(k)| \cdot n_c \quad (5)$$

$$n_x = |S_{x1}(k-1) - S_{x1}(k)| + |S'_{x2}(k-1) - S'_{x2}(k)| \quad (6)$$

where v_c^* is the reference and v_c^P is the predicted load voltage. v_{dc1}^P and v_{dc2}^P are the predicted DC-link voltages, which need to be kept at minimum difference to ensure a safe operation of the converter. There are two weighting factors λ_t and λ_{dc}, which can be adjusted using one of the weighting factor tuning techniques [15]. In the presented case study $\lambda_{dc} = 1$ and $\lambda_t = 0.07$ were used. The criterium for selected weights was an optimum trade off of low load voltage distortion, neutral point balance and minimum junction temperature difference of the active devices. Expression g_t has the purpose of controlling the switching losses in a way so the switching actions $S_x(k)$ are avoided during high current (I_{fx}) intervals in the converter phases $x \in a, b, c$. This is possible due to the use of redundant switching states of the NPC converter i.e. different switching combinations can be used to produce the same voltage vector (v_i). As seen from the cost function and prediction model, the control strategy does not require a junction temperature feedback. Instead, the thermal balance is realized only by controlling the switching frequency. It should be mentioned that the g_t objective will negatively affect the THD of the output voltage. However, the THD is not significantly increased as it will be demonstrated later and the positive effect on the converter lifetime is significant.

III. Thermal Stress Analysis

To analyse the thermal stress applied on the devices of the NPC converter, a simulation model was created in *Simulink*. The system parameters are given in Table I and the devices were modelled in *Plecs* using the data sheet values provided by the manufacturer [16]. Using the simulation model, for different ambient temperatures (T_a) and load demands (P_{load}), a look-up table was created. Afterwards it was used to translate

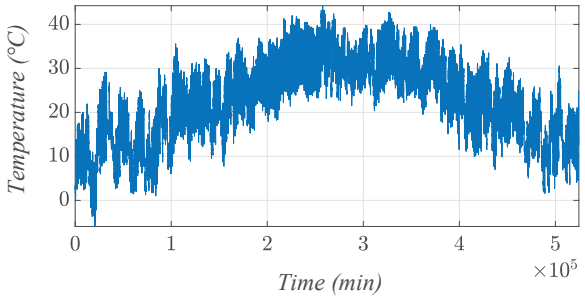

(a) Yearly temperature profile.

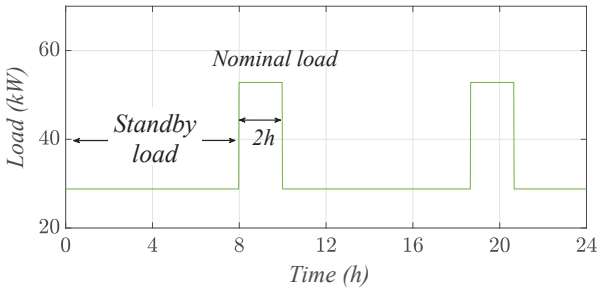

(b) Daily load demand profile (MP1).

Fig. 3: UPS mission profile (sampling resolution 60 s) used for lifetime estimation of NPC converter devices.

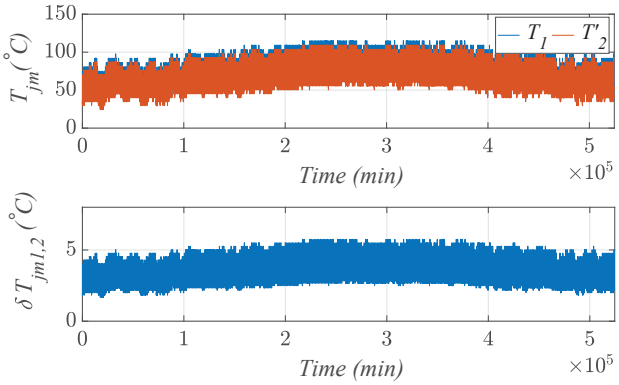

(a) Without active thermal control ($\lambda_t = 0$).

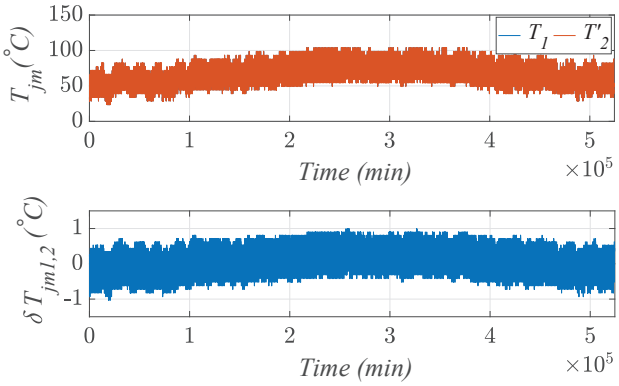

(b) With active thermal control ($\lambda_t = 0.07$).

Fig. 4: Power device junction temperatures (T_{jm}) and junction temperatures difference ($\delta T_{jm} = T_{jm\,1} - T'_{jm\,2}$) of the NPC converter for the yearly UPS mission profile.

the mission profile to the stress of the components. As mentioned in the introduction, the focus will be put on the IGBT devices and their failure mechanisms. In Fig. 3 the ambient temperature and the load demand profile for the UPS system can be observed. The load profile represents a typical backup power application with short periods of nominal demand and long periods of standby operation. The daily loading profile shown in Fig. 3b is repeated through the year.

For the presented mission profile, we can see in Fig. 4 how the junction temperature and the difference between the junction temperatures of the outer and inner IGBT are effected by applying the thermal balancing objective in the MPC cost function. Since the distribution is symmetrical, the figures show just one pair of the devices in the top half of the module. Also due to the symmetrical load, the distribution is equivalent in all three phases. When $\lambda_t = 0$ i.e. the stress distribution is not regulated and the difference in the temperature of the devices ($\delta T_{jm1,2}$) is almost $6°C$, while for $\lambda_t = 0.07$ this difference is reduced below $1°C$. If the temperature swing $\Delta T_{j1,2}$ of the devices is observed in Fig. 5a, it is evident that the outer devices have almost 3° C higher temperature swing than the inner devices. As shown in Fig. 5b when the proposed control algorithm is implemented, the temperature swing of the devices is almost equal.

IV. Lifetime Estimation Based on Mission Profile

Following the mission profile based lifetime estimation flow-chart presented in Fig. 6, the obtained junction temperatures from the previous analysis were used to calculate the damage of the IGBTs caused by the low frequency (LF) thermal cycling and the damage caused by the fundamental frequency (FF) power cycling. For the latter one, using the temperature swing (ΔT_j), minimum junction temperature ($T_{j,min}$) from the stress profile and heating time $t_{on} = 0.01$ the number of cycles to failure (N_f) can be calculated using the Bayerer lifetime model for IGBTs given in (7). From the remaining parameters, V_C is the blocking voltage of the chip, I_B is the current per bondwire, D is the bond wire diameter, A and β_1, β_2, β_3, β_4, β_5 and β_6 are constant parameters related to the specific IGBT devices. [17]

$$N_f = A \cdot \Delta T_j^{\beta_1} exp\left(\frac{\beta_2}{(T_{j,min} + 273)}\right) \cdot t_{on}^{\beta_3} \cdot I_B^{\beta_4} \cdot V_C^{\beta_5} \cdot D^{\beta_6} \quad (7)$$

The lifetime model (7) is obtained by performing the power cycling tests on the 4th generation of IGBT modules in [17]. For the lifetime model parameters the limits are provided in [18]. Recently, power cycling results were also published for low temperature swings (ΔT_j) and low heating time (t_{on}) in [19], [20]. The power cycling tests under these conditions are time consuming, as the device requires a lot of power cycles before the bondwire lift-off or chip solder layer degradation will occur. The preliminary results show that the number of

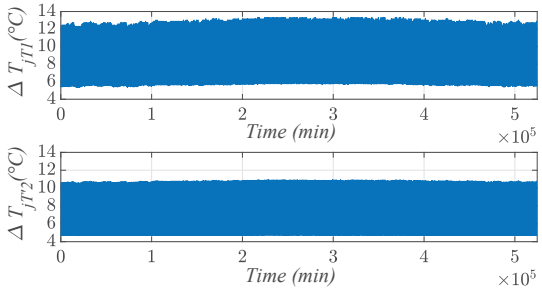

(a) Without thermal balancing control

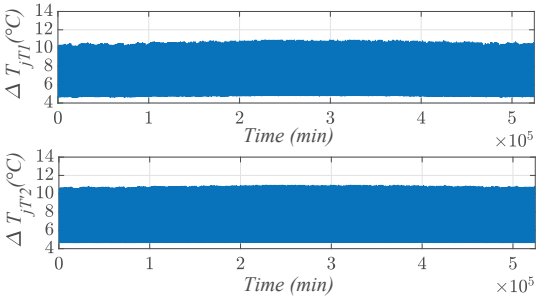

(b) With thermal balancing control

Fig. 5: Junction temperature swing of T_{1a} and T'_{a2}

cycles to failure at low temperature cycles is underestimated by (7), also the cycles with low ΔT_j may cause elastic deformation, which is reversible in the power devices. The authors of [20] stress that further work is still required to provide a lifetime model for low temperature swings. Thus, until a new lifetime model is provided that can accurately capture the device wear-out at low temperature swings, the authors would like to put more into the focus the relative improvement of the lifetime that the active thermal control can provide, rather than absolute lifetime values.

For calculating the damage due to low frequency thermal cycling, a rainflow algorithm needs to be used to extract the ΔT_j, $T_{j,min}$, t_{on} and the number of cycles (n_i), before using the lifetime model. Once N_f is obtained for all stress conditions i, Miner's rule (8) can be applied to calculate the accumulated damage (LC) i.e. how much of the device's lifetime is consumed during the operation of the converter for a given mission profile.

$$LC = \sum_i \frac{n_i}{N_{fi}} \tag{8}$$

A. Monte Carlo simulations

All lifetime models have an uncertainty, which originates in the variance of the device manufacturing process or the variance in the lifetime model fitting parameters. In the lifetime estimation process both uncertainties were implemented. To take into account the variation of the IGBT parameters and uncertainty of the lifetime model fitting parameters, Monte Carlo simulations were used. While the variation intervals of the lifetime model constants ($\beta_1 - \beta_2$) are given in [17],

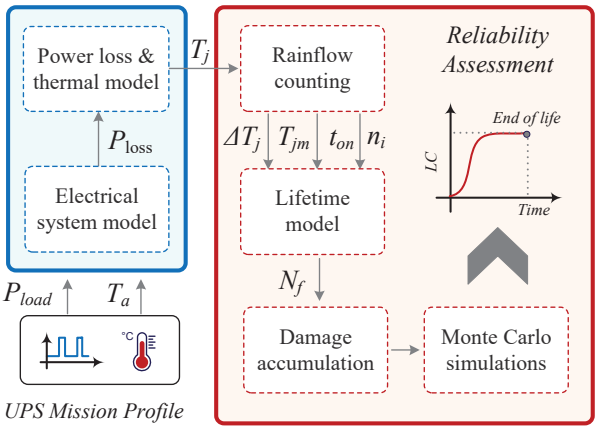

Fig. 6: Mission profile based lifetime estimation (LC is accumulated damage).

for the mission profile parameters ΔT_j and $T_{j\,min}$ a normal distribution with a variation range of 5% was used. [11] These variations were applied to a static mission profile parameters, which are equivalent to the dynamic profile in Fig. 3. [21]

The parameters of the static mission profile for the NPC converter without the thermal balancing control are given in Table II. The temperature swing ΔT_j caused by the ambient temperature is two times higher than for the fundamental frequency, however the number of cycles n is significantly lower. In Table III static parameters were also obtained for the NPC converter with the thermal balancing control. It can be noticed that the temperature swing for both cycles is almost equal for the two devices and the accumulated damage LC is reduced for the outer device compared to outer device LC given in Table II. Thus, the thermal balancing control has a positive impact on both cycle types.

The Monte Carlo analysis is performed on a population of 10 000 samples for the lifetime model (7) to obtain the probability density function (*pdf*) of the accumulated damage. The *pdf* can be fitted to a Weibull distribution:

$$f(x) = \frac{\beta}{\eta^\beta} x^{\beta-1} exp\left[-\left(\frac{x}{\eta}\right)^\beta \right] \tag{9}$$

where β is the shape parameter, η is the scale parameter and x is the operation time. η parameter also corresponds to the time when 63.2% of the population have failed and β parameter represents the failure mode. $\beta > 1$ indicates increasing failure rate and it is associated with the wear-out leading to end of life of the component [22]. For the obtained *pdf* plots in Fig. 7 it is shown that the devices have a similar failure mode (β) and that the time when 63.2% of the population will fail is two times shorter for the outer device without thermal balancing control than for the other devices.

B. System unreliability for MP1

After obtaining the Weibull *pdf* functions for all three devices, the reliability of the components and the system can be evaluated using the cumulative density function *cdf* of the

TABLE II: Equivalent static parameters used in Monte Carlo simulations for the two cycle types (FF: fundamental frequency , LF: low frequency).

Par.	T_1		T_2	
	FF	LF	FF	LF
$T_{j\,min}$	59.6°C	59.6°C	57.1°C	57.1°C
ΔT_j	9.5°C	19.4°C	7.9°C	18.3°C
LC	0.05	0.0016	0.0216	0.0012
n	$1.6{\cdot}10^9$	2904	$1.6{\cdot}10^9$	2904
N_f	$3.1{\cdot}10^{10}$	$1.8{\cdot}10^6$	$7.3{\cdot}10^{10}$	$2.4\cdot10^6$

TABLE III: Equivalent static parameters used in Monte Carlo simulations for the two cycle types (FF: fundamental frequency , LF: low frequency).

Par.	T_1		T_2	
	FF	LF	FF	LF
$T_{j\,min}$	55.6°C	55.6°C	55.3°C	55.3°C
ΔT_j	7.8°C	16.7°C	7.8°C	17°C
LC	0.02	0.0076	0.02	0.0083
n	$1.6{\cdot}10^9$	2904	$1.6{\cdot}10^9$	2904
N_f	$7.8{\cdot}10^{10}$	$3.8{\cdot}10^5$	$7.8{\cdot}10^{10}$	$3.5{\cdot}10^5$

obtained Weibull distribution. The *cdf* ($F(x)$) is obtained by integrating the Weibull distribution $f(x)$ over the time x. For the NPC converter the system unreliability was obtained using the following equation:

$$F_{sys}(x) = 1 - (1 - F_{T_1}(x))^6 (1 - F_{T_2'}(x))^6 \qquad (10)$$

where $F_{T_1}(x), F_{T_2'}(x)$ are the unreliability functions of the inner and outer IGBT device. In this equation it is assumed that: 1) the NPC system has failed if one of the 12 devices fails (i.e. we assume a series connection of all devices in the reliability block diagram), 2) the loading conditions in each phase are equivalent and 3) symmetrical loading in each phase. Therefore, in each phase there are two pairs of devices with the equivalent thermal stress, the *cdf* functions for the devices can be raised to the power of 6 in the equation (10). Due to unidirectional power flow of the UPS configuration in this paper, the diodes in the NPC topology are not experiencing any high thermal loading like the active switches. Therefore, the analysis is simplified to only include the active devices (T_1, T_2), which significantly contribute to the lifetime consumption of the NPC converter. The unreliability functions for NPC system are shown in Fig. 8.

Another parameter that is used to specify the reliability is the B_x-lifetime. This is the time by which a certain percent (x) of the population will fail [22]. This means that a B_1-lifetime of 4.2 years for the NPC converter with thermal balancing control is equivalent to 99% reliability for 4.2 years of mission life. The obtained B_x-lifetime confirm the trend that was already observed in the *pdf* plots in Fig. 7. The expected B_x lifetime for the system without thermal balancing control

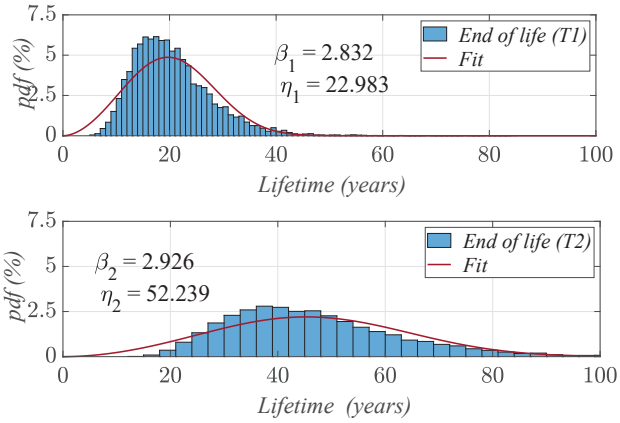

(a) Without thermal balancing control

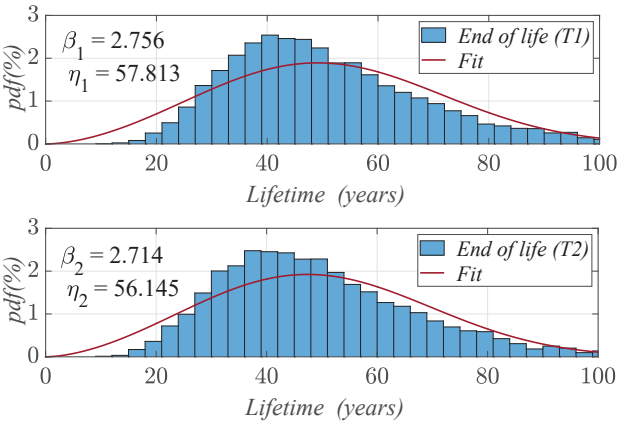

(b) With thermal balancing control

Fig. 7: End of life distribution for T_{1a} and T'_{a2} without and with thermal balancing control.

is two times lower then when the thermal balancing control is included.

C. System unreliability for different mission profiles

To further increase the reliability of the converter we could either increase the converter heatsink size or modify the loading conditions of the converter. To illustrate the impact of the different loading conditions on the UPS system, three more load mission profiles were defined like shown in Fig. 9. The ambient temperature profile T_a is the same as for MP1 (see Fig. 3a). It is observed that each of the profiles has a different combination of the standby and nominal loading conditions. The conditions are also summarized in Table IV.

The workflow for the mission profile based lifetime estimation from Fig. 6 was repeated for the new mission profiles. A comparison of the obtained system unreliability functions with the previously presented (MP1) is shown in Fig. 10 and the expected B_1 lifetime calculations are included in Table IV. It is observed that both the standby and high load conditions have a high impact on the B_1 lifetime. For the mission profile with standby load that equals the 25% of the nominal converter load and the high load conditions that equal the 80% of the nominal converter load, the B_1 lifetime is increased five times,

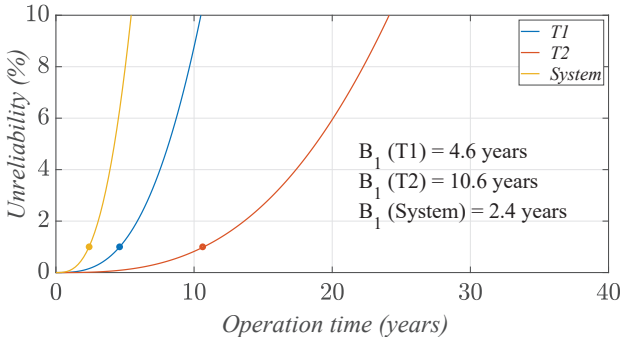

(a) Without thermal balancing control

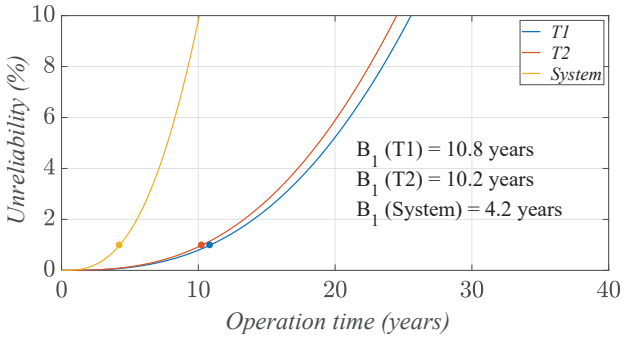

(b) With thermal balancing control

Fig. 8: Unreliability function of T_{1a}, T'_{a2} and the NPC converter without and with thermal balancing control.

which would make it suitable for an UPS application with a high reliability demand. It also should be mentioned that B_1 is a rather conservative approach since the B_{10} lifetime (10% failed converters) is commonly used [23].

V. Conclusion

A control strategy with active thermal control to balance the device loading can significantly increase the lifetime of NPC converters used in UPS applications. The selected model predictive control algorithm with active thermal control can maintain the thermal stress balance during a typical UPS mission profile with a lot of variance in the ambient temperature. The temperature difference between the inner and outer devices is reduced from 5°C to 1°C. This is also reflected in the the B_1 system lifetime, which is two times higher if the NPC converter is using the active thermal control.

The obtained device lifetime estimations for different load mission profiles confirm that the selected topology with the proposed control can provide a high B_1 lifetime for UPS applications if the standby and high loading condition of the converter are defined as 25% of the nominal converter load for the standby operation and 80% of the nominal converter load for the high load operation.

Acknowledgement

The work is supported by the Reliable Power Electronic-Based Power System (REPEPS) project at the Department of Energy Technology, Aalborg University as a part of the Villum Investigator Program funded by the Villum Foundation.

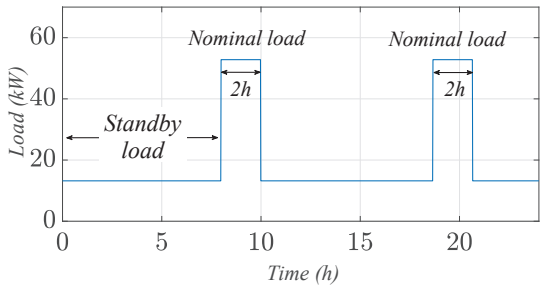

(a) MP2 - Standby load (25% nominal load) .

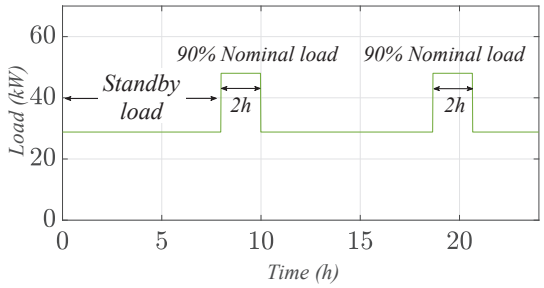

(b) MP3 - Standby load (50% nominal load).

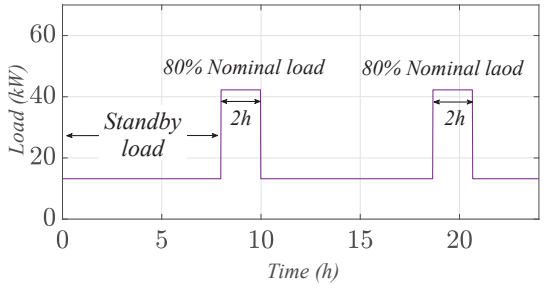

(c) MP4 - Standby load (25% nominal load).

Fig. 9: Daily load demand UPS mission profiles (MP) used for lifetime estimation of NPC converter devices (nominal load = 53 kW).

References

[1] K. Ma, H. Wang, and F. Blaabjerg, "New approaches to reliability assessment: Using physics-of-failure for prediction and design in power electronics systems," *IEEE Power Electron. Magazine*, vol. 3, no. 4, pp. 28–41, Dec 2016.

[2] J. Rodriguez, S. Bernet, P. K. Steimer, and I. E. Lizama, "A survey on neutral-point-clamped inverters," *IEEE Trans. Ind. Electron.*, vol. 57, no. 7, pp. 2219–2230, July 2010.

[3] K. Ma and F. Blaabjerg, "Modulation methods for neutral-point-clamped wind power converter achieving loss and thermal redistribution under low-voltage ride-through," *IEEE Trans. Ind. Electron.*, vol. 61, no. 2, pp. 835–845, Feb 2014.

[4] M. Aly, G. M. Dousoky, E. M. Ahmed, and M. Shoyama, "A unified SVM algorithm for lifetime prolongation of thermally-overheated power devices in multi-level inverters," in *Proc. IEEE Energy Conversion Congress and Exposition (ECCE)*, Sept 2016, pp. 1–6.

[5] M. Aly, E. M. Ahmed, and M. Shoyama, "Thermal stresses relief carrier-based PWM strategy for single-phase multilevel inverters," *IEEE Trans. Power Electron.*, vol. 32, no. 12, pp. 9376–9388, Dec 2017.

TABLE IV: Results of a finite-set MPC controlled three level NPC converter in standalone application for different load profiles. P_n is the rated nominal load of the converter. ATC: Active Thermal Control.

Mission profile	Nominal load	Standby load	B_1 without ATC	B_1 with ATC	Lifetime improvement
MP1	53 kW (P_n)	29 kW (55% of P_n)	2.4 years	4.2 years	75%
MP2	53 kW (P_n)	13 kW (25% of P_n)	2.2 years	4 years	82%
MP3	48 kW (90% of P_n)	29 kW (55% of P_n)	4.6 years	8.4 years	83%
MP4	42 kW (80% of P_n)	13 kW (25% of P_n)	11 years	19 years	73%

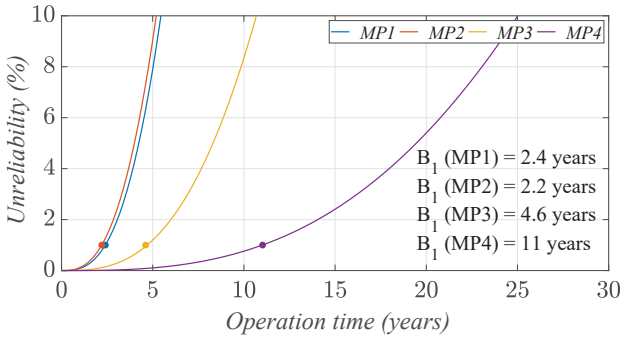

(a) Without thermal balancing control

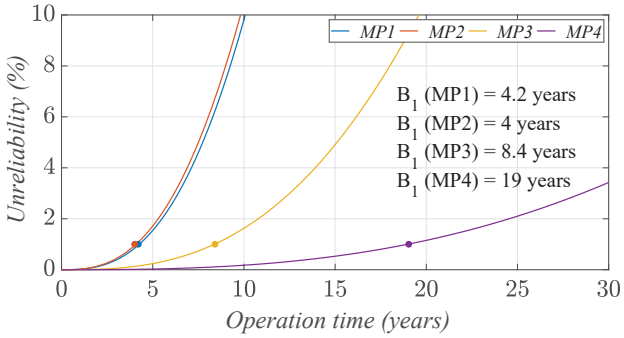

(b) With thermal balancing control

Fig. 10: Unreliability functions for NPC converter with different mission profiles, without and with thermal balancing control.

[6] J. Zhou and P. Cheng, "Modulation methods for 3l-npc converter power loss management in statcom application," *IEEE Trans. Ind. Appl*, vol. 55, no. 5, pp. 4965–4973, Sep. 2019.

[7] Q. Chen, Z. Chen, Q. Wang, G. Li, and L. Cheng, "Analyze and improve lifetime in 3l-npc inverter from power cycle and thermal balance," in *Proc. of ICEMS 2014*, Oct 2014, pp. 974–980.

[8] F. Richardeau and T. T. L. Pham, "Reliability calculation of multilevel converters: Theory and applications," *IEEE Trans. Ind. Electron.*, vol. 60, no. 10, pp. 4225–4233, Oct 2013.

[9] M. Boettcher, J. Reese, and F. W. Fuchs, "Reliability comparison of fault-tolerant 3l-npc based converter topologies for application in wind turbine systems," in *Proc. of IECON 2013*, Nov 2013, pp. 1223–1229.

[10] V. de Nazareth Ferreira, A. Fagner Cupertino, H. Augusto Pereira, A. Vagner Rocha, S. Isaac Seleme, and B. de Jesus Cardoso Filho, "Design and selection of high reliability converters for mission critical industrial applications: A rolling mill case study," *IEEE Trans. Ind. Appl.*, vol. 54, no. 5, pp. 4938–4947, Sep. 2018.

[11] A. Sangwongwanich, Y. Yang, D. Sera, and F. Blaabjerg, "Mission profile-oriented control for reliability and lifetime of photovoltaic inverters," *IEEE Trans. Ind. Appl.*, vol. 56, no. 1, pp. 601–610, Jan 2020.

[12] D. Zhou and F. Blaabjerg, "Converter-level reliability of wind turbine with low sample rate mission profile," *IEEE Transactions on Industry Applications*, vol. 56, no. 3, pp. 2938–2944, 2020.

[13] D. Zhou, H. Wang, and F. Blaabjerg, "Mission profile based system-level reliability analysis of dc/dc converters for a backup power application," *IEEE Trans. Power Electron.*, vol. 33, no. 9, pp. 8030–8039, Sep. 2018.

[14] M. Novak, T. Dragicevic, and F. Blaabjerg, "Finite set mpc algorithm for achieving thermal redistribution in a neutral-point-clamped converter," in *Proc. of IECON 2018*, Oct 2018, pp. 5290–5296.

[15] P. Karamanakos and T. Geyer, "Guidelines for the design of finite control set model predictive controllers," *IEEE Transactions on Power Electronics*, vol. 35, no. 7, pp. 7434–7450, 2020.

[16] *3-Level NPC IGBT-Module: SKiiP 28MLI07E3V1 datasheet*, Semikron, 6 2016, rev. 1.0.

[17] R. Bayerer, T. Herrmann, T. Licht, J. Lutz, and M. Feller, "Model for power cycling lifetime of IGBT modules - various factors influencing lifetime," in *Proc. of CIPS*, 2008, pp. 1–6.

[18] W. T. A. Wintrich, U. Nicolai and T. Reimann, *Application Manual Power Semiconductors*, 2nd ed. SEMIKRON International GmbH, 2015.

[19] G. Zeng, R. Alvarez, C. Kunzel, and J. Lutz, "Power cycling results of high power igbt modules close to 50 hz heating process," in *2019 21st European Conference on Power Electronics and Applications (EPE '19 ECCE Europe)*, 2019, pp. 1–10.

[20] J. Lutz, C. Schwabe, G. Zeng, and L. Hein, "Validity of power cycling lifetime models for modules and extension to low temperature swings," in *2020 22st European Conference on Power Electronics and Applications (EPE '20 ECCE Europe)*, 2020, pp. 1–9.

[21] J. W. Mcpherson, *Reliability Physics and Engineering: Time-To-Failure Modeling*, 3rd ed. Springer International Publishing, 2019.

[22] P. P. O'Connor and A. Kleyner, *Practical Reliability Engineering*, 5th ed. Wiley Publishing, 2012.

[23] J. Berner, "Load-cycling capability of hipak igbt modules," in *ABB Application Note 5SYA 2043-02*, 2012, pp. 1–8.